tvst

Article

Predicting Age From Optical Coherence Tomography Scans With Deep Learning

Leonardo S. Shigueoka[1,2], Eduardo B. Mariottoni[1], Atalie C. Thompson[1], Alessandro A. Jammal[1,2], Vital P. Costa[2], and Felipe A. Medeiros[1]

[1] Vision, Imaging and Performance Laboratory (VIP), Duke Eye Center and Department of Ophthalmology, Duke University, Durham, NC, USA

[2] Glaucoma Service, Department of Ophthalmology, University of Campinas, Campinas, Saō Paulo, Brazil

Correspondence: Felipe A. Medeiros, Duke Eye Center, Department of Ophthalmology, Duke University, 2351 Erwin Rd, Durham, North Carolina, 27705, USA. e-mail: felipe.medeiros@duke.edu

Purpose: To assess whether age can be predicted from deep learning analysis of peripapillary spectral-domain optical coherence tomography (SD-OCT) B-scans and to determine the importance of specific retinal areas on the predictions.

Methods: Deep learning (DL) convolutional neural networks were developed to predict chronological age in healthy subjects using peripapillary SD-OCT B-scan images. Models were built using the whole B-scan, as well as using specific regions through image ablation. Cross-validation was used for training and testing the model. Mean absolute error (MAE) and correlations between predicted and observed age were used to evaluate model performance.

Results: A total of 7271 images from 542 eyes of 278 healthy subjects were included. DL predictions of age using the whole B-scan were strongly correlated with chronological age (MAE = 5.82 years; $r = 0.860$, $P < 0.001$). The model also accurately discriminated between the lowest and highest tertiles of age, with an area under the receiver operating characteristic curve of 0.962. In general, class activation maps tended to show a diffuse pattern of activation throughout the scan image. For specific structures of the B-scan, the layers with the strongest correlations with chronological age were the choroid and vitreous (both $r = 0.736$), whereas retinal nerve fiber layer had the lowest correlation ($r = 0.492$).

Conclusions: A DL algorithm was able to accurately predict age from whole peripapillary SD-OCT B-scans.

Translational Relevance: DL models applied to SD-OCT scans suggest that aging appears to affect several layers in the posterior eye segment.

Introduction

Spectral-domain optical coherence tomography (SD-OCT) is a noninvasive technology able to provide high-resolution images of retinal structures based on interferometric analysis of low-coherence light.[1] Because progressive retinal damage is a hallmark of certain eye diseases, such as glaucoma and age-related macular degeneration, identification of SD-OCT structural changes over time is fundamental for the diagnosis and monitoring of these conditions.[2–5] However, detection of pathologic damage relies funda-mentally on the ability to differentiate it from normal, age-related structural changes. Although many different tissues of the posterior segment of the eye seem to be affected by aging,[6–17] a precise identification of the age-related structural changes on SD-OCT is still lacking. Although some studies have focused on the impact of aging on the thicknesses of specific layers, such as the retinal nerve fiber layer (RNFL)[6–14] or the choroid,[15–17] it is conceivable that aging may also affect other tissue properties. However, without knowing a priori which properties or image characteristics could be affected, it becomes difficult to investigate the true impact of age using traditional methods.

In recent years, deep leaning (DL) with convolutional neural networks has become the go-to algorithm for computer vision tasks, such as image classification, object detection, and segmentation,[18] achieving and sometimes surpassing human-level performance.[19,20] These techniques have been applied to produce highly accurate algorithms able to detect diseases such as age-related macular degeneration, diabetic retinopathy,[21,22] and glaucoma[23–26] from medical images.[27] An important and appealing characteristic of DL networks is that they do not require manual definition of features from an image to succeed in performing a task. The network learns automatically to extract the most relevant features during training, so that only the raw image needs to be fed as an input. This makes these networks suitable to address the question of which retinal layers and image characteristics of an SD-OCT scan are mostly affected by age.

In this study, we used DL models to investigate characteristics associated with normal aging on SD-OCT B-scans. We hypothesized that a DL algorithm could be successfully trained to predict age from peripapillary SD-OCT B-scans. We also hypothesized that the impact of aging on the different layers of the retina, choroid, and vitreous could be ascertained by image ablation, that is, using DL networks trained to predict age from SD-OCT scans that had specific layers removed.

Methods

Participants from this study were drawn from the Duke Glaucoma Registry (DGR), a database of research and clinical patients collected by the Vision, Imaging and Performance (VIP) Laboratory at the Duke Eye Center. All SD-OCT images and data were deidentified according to the Health Insurance Portability and Accountability Act. The study adhered to the tenets of the Declaration of Helsinki for human subject research and was approved by the Duke University institutional review board.

Participants were healthy subjects older than 18 years and had completed a comprehensive ophthalmologic examination, which included review of medical history, diagnosis, visual acuity, intraocular pressure measurements, gonioscopy, as well as anterior segment and dilated slit-lamp exam. All patients underwent SD-OCT imaging (Spectralis, Heidelberg Engineering, Dossenheim, Germany) and standard automated perimetry (SAP; Humphrey Field Analyzer II and III; Carl Zeiss Meditec, Inc., Dublin, CA, USA) that was acquired with the 24-2 or 30-2 Swedish Interactive Threshold Algorithm. Visual fields were excluded if they had more than 33% fixation losses or more than 15% false-positive errors. Patients were excluded if they had any history of ocular or systemic diseases that could affect the retina, optic nerve or the visual field.

Peripapillary circular B-scans, consisting of 1536 A-scans from a 3.45 mm circle centered on the optic disc were acquired on all subjects from multiple timepoints during follow-up. The device's eye-tracking capability was used during image acquisition to adjust for eye movements and to ensure that the same location of the retina was scanned over time. Images were reviewed manually to ensure quality and scan centration, and to ensure that there were no coexistent retinal pathologies or artifacts. The signal strength ranged from 0 (poor) to 40 decibels (excellent). Images that had a signal strength below 15 were excluded.[28–30] From a total of 7836 images available, there were 565 (7.21%) images excluded because of poor quality, decentration, segmentation errors, or other artifacts.

Deep Learning Algorithm to Predict Age

A convolutional neural network was trained to predict age from the peripapillary SD-OCT B-scan images. For training and testing, we used the standard machine learning approach of fivefold cross-validation. The 7271 available images from 542 eyes of 278 subjects were randomly split at the participant level into five equally sized folds. We used three folds for training, one fold for validation (to optimize the hyperparameters and select the best set of weights), and the remaining fold for testing. This process was repeated five times, reserving a different fold each time as the testing set. These settings allowed us to evaluate the model using the whole sample to improve generalizability of the results. Randomization at the subject level was important to guarantee that no subject was present in more than one fold to prevent leakage and biased estimates of test performance. We used a residual deep neural network (ResNet50) architecture[31] that had been pretrained to classify images in the ImageNet dataset.[32] To adapt the network's architecture to predict the patient's age at the time of the SD-OCT scan, the last layer was replaced to produce a single continuous output. The training was performed with stochastic gradient descent, with minibatches of size 64 and Adam optimizer.[33,34] Initially, only the top two layers were trained, without adjusting the weights of the bottom layers. Subsequently, all layers were unfrozen, and additional training was performed using differential learning rates, in which a lower learning rate

is used for the bottom layers and a gradually increasing learning rate is used for the later layers. The best learning rate was found using the cyclical learning method with stochastic gradient descent with restarts.[35]

To investigate the impact of different ocular structures represented in the SD-OCT peripapillary scan on the predictions of age, we trained additional models to predict age using specific regions of the B-scan: (a) vitreous, (b) RNFL, (c) the remaining retina layers, and (d) choroid. For each model, the region of interest remained unchanged, while the rest of the image was ablated, that is, removed by replacing it with a black mask. The performances of the different models were used as a proxy of how much information related to aging could be extracted from each region.

We also investigated the ability of the DL models to discriminate the oldest from the youngest subjects using SD-OCT scans. For this analysis, the sample was divided into tertiles according to age, with the lowest (i.e., youngest) and highest tertiles (i.e., oldest) of age retained. Gradient-weighted class activation maps[36] were built to assess which parts of the SD-OCT scan were most relevant in discriminating between the two groups.

Statistical Analyses

Pearson's correlation coefficient (r) and mean absolute error (MAE) were used to assess how well the DL models were able to predict chronological age. The area under the receiver operating characteristic (ROC) curve (AUC) was used to assess the accuracy of the DL model in discriminating the oldest from the youngest subjects. Due to the fact that multiple images were used from each participant, nonparametric bootstrap resampling procedures were used to derive confidence intervals (CI) and *P* values, where the cluster of data for the participant was considered as the unit of resampling to adjust standard errors. This procedure has been used previously to adjust for the presence of multiple correlated measurements from the same unit.[37]

Multivariable linear regression models were built to account for the effect of confounders, such as signal strength, on the relationship between the DL predictions of age from SD-OCT images and the actual observed chronological age. Generalized estimating equations were used to account for the hierarchical and unbalanced nature of the data.[38] The α level (type I error) was set at 0.05. Statistical analyses were performed with Stata (version 16; StataCorp, College Station, TX, USA).

Table 1. Demographic and Clinical Characteristics of the Eyes and Participants Included in the Study

	Total
No. of images	7271
No. of eyes	542
No. of participants	278
Age (years)	
mean $\pm$ SD	55.8 $\pm$ 14.1
range	20.8 to 85.8
Female gender (%)	66.4
Race (%)	
Caucasian	67.5
Black or African American	25.4
Asian	3.7
Other	3.4
SAP MD (dB), mean $\pm$ SD	0.07 $\pm$ 1.3
SAP PSD (dB), mean $\pm$ SD	1.6 $\pm$ 0.4
SD-OCT global RNFL thickness (μm), mean $\pm$ SD	96.9 $\pm$ 9.9

MD, mean deviation; PSD, pattern standard deviation; SAP, standard automated perimetry.

Results

The overall dataset included 7271 peripapillary SD-OCT B-scans from 542 eyes of 278 healthy participants. The mean age of the study sample was 55.8 $\pm$ 14.1 years. Table 1 summarizes demographic information and clinical data.

DL predictions of age from whole SD-OCT B-scans were highly correlated with the true chronological age ($r = 0.860$, $R^2 = 74\%$, $P < 0.001$), with a MAE of 5.82 years. Figure 1 shows a scatterplot of
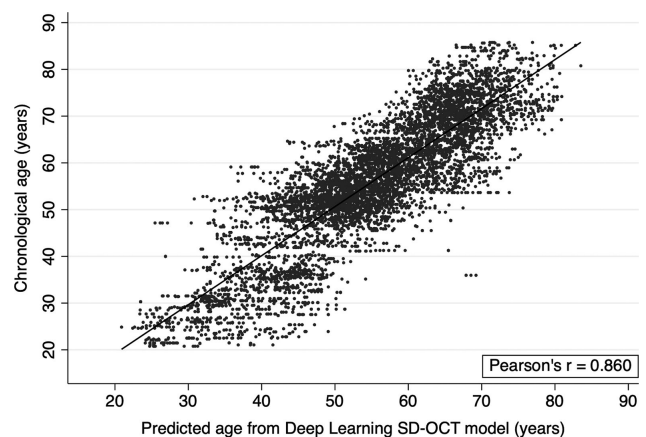
Figure 1. Scatterplot showing the relationship between predicted age from the deep learning model applied to the whole SD-OCT peripapillary B-scan versus the true chronological age on the study dataset.
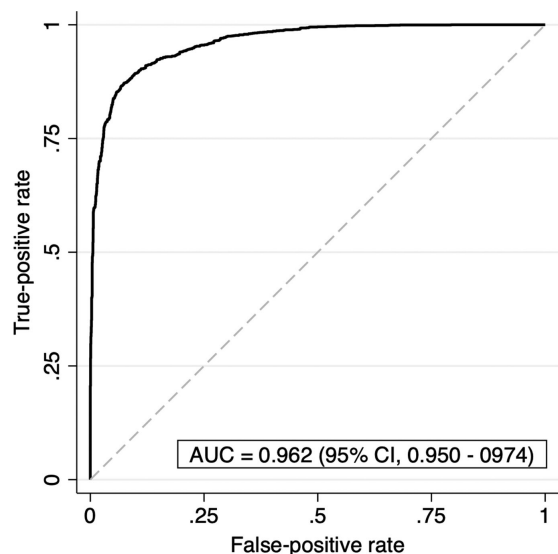
Figure 2. AUC and confidence interval (CI) for the deep learning algorithm in discriminating between oldest and youngest tertiles.

predicted versus actual age values. For discrimination of the oldest versus youngest tertiles, the DL model using the whole B-scan had an AUC of 0.962 (95% CI: 0.950 to 0.974) (Fig. 2). Figure 3 shows class activation maps (heatmaps) for the DL algorithm for scans that were correctly classified into the youngest versus oldest tertiles and examples of predictions with large absolute errors. Of note, the heatmaps of scans that were correctly classified showed a diffuse activation of all layers in the retina and choroid. On manual inspection, no specific layer seemed of greater importance for the classification decision. For the scans that were correctly classified in the younger group, the posterior vitreous was also generally highlighted as an important area for the classification decision. The heatmaps of images that had large prediction errors did not appear to show a diffuse pattern but rather seemed to highlight localized regions of the scan, although by manual inspection it was not possible to identify the characteristics of the image that were more relevant for the classification.

We then retrained the DL networks using image ablation to obtain further insight into the regions of the scan that were most relevant for age prediction. When trained and applied to the ablated B-scans for isolating specific regions (i.e., vitreous, RNFL, choroid, and all retinal layers except for the RNFL) the DL algorithm also yielded age predictions with significant correlations with the actual age and MAE ranging from 7.56 to 9.99 years. Figure 4 summarizes the performance of the various DL models and illustrates an example of a B-scan with the whole image and the structural areas of interest in isolation. The correlation between the

chronological age and the DL predicted age was significantly greater for the DL algorithm using the whole B-scan than the correlations for DL algorithms applied to isolated regions of the scan (Table 2). Interestingly, the weakest prediction was observed for SD-OCT scans that had only the RNFL, with MAE of 9.99 years and a significantly lower correlation ($r = 0.492$, $R^2 = 24\%$) compared to all other structural areas (Table 2).

Of note, signal strength measurements from the SD-OCT B-scans were statistically significantly associated with true chronological age in univariable analysis ($r = -0.77$; $P < 0.001$). To assess whether signal strength could act as a confounder in the association between DL predictions and observed age, we included signal strength in a multivariable model for predicting chronological age, along with the DL predictions. The DL predictions remained statistically significantly associated with observed age ($P < 0.001$), whereas signal strength ($P = 0.919$) was no LONGER significantly associated with age in the multivariable model.

Discussion

In the current study, we were able to estimate chronological age using a DL algorithm trained on peripapillary SD-OCT B-scan images of healthy adult subjects. The ability to accurately predict age was superior when the entire B-scan image was used in the algorithm in comparison to when individual regions were used. Moreover, we found that changes in multiple peripapillary structures on the SD-OCT B-scan seem to be more important to predict age than RNFL itself.

DL algorithms have previously been used to investigate structural changes related to normal aging using other imaging methods. Poplin et al.[20] developed a DL algorithm that was able to predict age and other cardiovascular risk factors from color fundus photographs. The algorithm achieved R^2 of 74% and 82% and MAEs of 3.26 and 3.42 years in predicting age in two independent test sets. In our study, using a DL model trained on raw peripapillary SD-OCT B-scan images, we achieved an identical R^2 of 74% for predicting chronological age, but with a higher MAE of 5.82 years. The larger MAE in our sample may perhaps be explained by the wider variability of age in our sample. Although the standard deviations of age in the subjects included in the test datasets of Poplin et al.[20] were 8.2 and 10.9 years, ours was 14.1 years. As Figure 1 shows, greater errors in the predictions were apparent in individuals younger than 50 years. Despite this fact, the DL algorithm in our study was still able to accurately discriminate between the oldest and youngest tertiles with an AUC of 0.962.

Correct predictions

Incorrect predictions

Age = 35.9
DL Age = 34.8

Age = 69.8
DL Age = 70.0

Age = 47.6
DL Age = 63.0

Age = 66.4
DL Age = 53.9
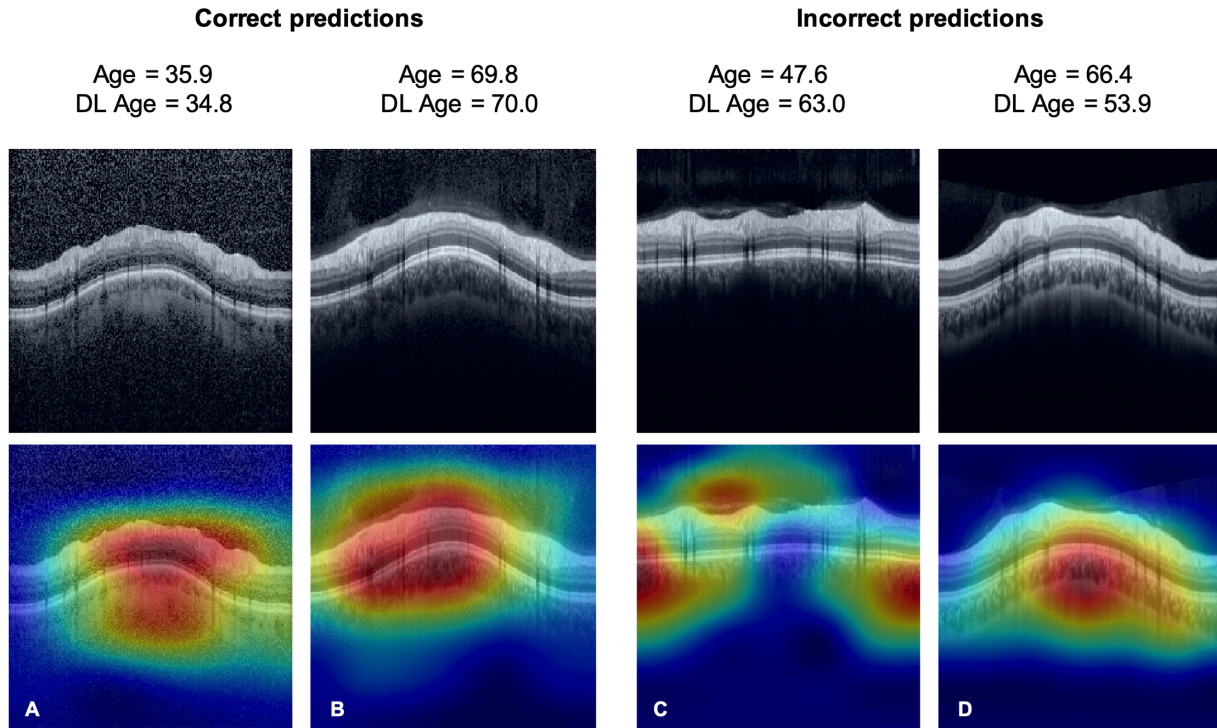
Figure 3. Examples from the age prediction and the class activation maps (heatmaps) showing the regions of the peripapillary spectral-domain optical coherence tomography B-scan images that had the greatest weight in the DL algorithm's discrimination between oldest versus youngest tertiles. The chronological age and the predicted age are reported above each image. (A) Individual correctly classified within the youngest tertile. (B) Individual correctly classified within the oldest tertile. (C) Young individual with an age prediction error (overestimation of true age) of 15.4 years. (D) Older individual that had an underestimated prediction of age by 12.5 years.

In the work by Poplin et al.,[20] they hypothesized that the appearance of the retinal vessels seemed to be the most important factor in their model's predictions of age. In fact, heatmaps of their model highlighted the blood vessels in the fundus photographs in 95% of the cases.[20] In our study, we found that the heatmaps tended to be more diffuse and involve several layers of the retina. While peripapillary SD-OCT B-scans do not contain clear information on the shape of retinal blood vessels, it is possible that the model could still be using information on the caliber of the vessels, as derived from the shadows cast by them in the scan. As another important consideration, it is possible that results of the model by Poplin et al.[20] could have been

Table 2. Comparison of Correlation Coefficients Between the Age Predictions from the Deep Learning Algorithms and the True Chronological Age Using the Entire B-Scan or the Different Isolated Areas

	Choroid	Vitreous	Retina[*]	RNFL
Entire B-scan	0.860 vs. 0.736 (0.006 to 0.155)	0.860 vs. 0.736 (0.071 to 0.267)	0.860 vs. 0.672 (0.061 to 0.305)	0.860 vs. 0.492 (0.307 to 0.418)
Choroid		0.736 vs. 0.736 (−0.058 to 0.219)	0.736 vs. 0.672 (−0.038 to 0.230)	0.736 vs. 0.492 (0.148 to 0.490)
Vitreous			0.736 vs. 0.672 (−0.135 to 0.137)	0.736 vs. 0.492 (0.042 to 0.425)
Retina[*]				0.672 vs. 0.492 (0.006 to 0.425)

The parentheses show 95% confidence interval of the difference.
[*]Retinal layers without the RNFL.

	SD-OCT structure used in DL algorithm	MAE (years)	Correlation to Chronological Age	
			Pearson's r [95% CI]	R² [95% CI]
	Entire B-scan	5.82	0.860 [0.854 – 0.866]*	0.740 [0.729 – 0.750]
	Vitreous	7.56	0.736 [0.725 – 0.748]*	0.542 [0.526 – 0.559]
	RNFL	9.99	0.492 [0.474 – 0.509]*	0.242 [0.225 – 0.259]
	Retinal Layers without the RNFL	8.32	0.672 [0.660 – 0.685]*	0.452 [0.436 – 0.469]
	Choroid	7.56	0.736 [0.724 – 0.748]*	0.542 [0.525 – 0.559]
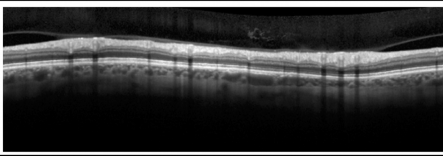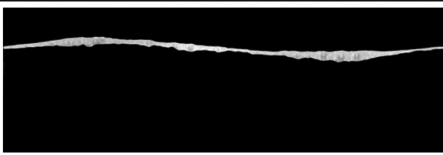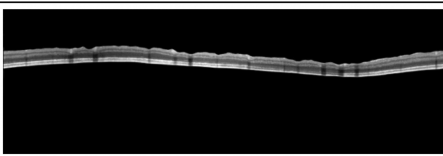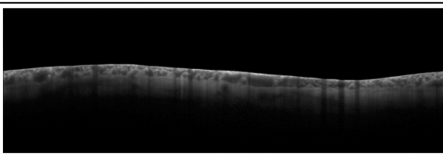
CI = confidence interval; DL = deep learning; MAE = mean absolute error; SD-OCT = spectral domain optical coherence tomography; RNFL = retinal nerve fiber layer. *P < 0.001

Figure 4. Results of deep learning models using image ablation for the different retinal structures.

confounded by issues of photographic quality. With aging, the decrease in media quality might lead to change in color, contrast, and brightness of fundus photos. Their model could be using such information to predict age, rather than true anatomic changes. Because they did not have an objective index to assess photographic quality, no adjustment could be done in their study. In contrast, we used signal strength to directly assess the impact of scan quality in the age predictions from our model. We observed that even after adjusting for signal strength, the DL model predictions were still significantly associated with chronological age.

Because multiple studies have suggested that global RNFL thickness declines with aging at a rate of approximately 0.2 to 0.5 µm per year,[8–13] we expected that the RNFL would be an important feature driving the DL algorithm's prediction of age. However, the model developed with images ablated to isolate the RNFL had a significantly weaker ability to predict chronological age, with $r = 0.492$ ($R^2 = 24\%$), compared to the model involving all layers. This is an interesting result as it might suggest on first look that the impact of age on RNFL is not as important. In fact, in a study by Fortune and colleagues[39] imaging Rhesus monkeys with SD-OCT and performing histologic counting of the optic nerve axons, the authors found only a small influence of age on axon count, with an R^2 lower than 1%. They suggested that a large proportion of the effect of aging on SD-OCT RNFL thickness could actually be explained by optical degradation of the aging eye reducing SD-OCT scan quality, as well as thinning of the major blood vessels. The issue of whether aging leads to retinal ganglion cell and axonal loss is controversial, with several other studies suggesting significant losses over time.[40–43] Regardless of whether age effects are explained by actual loss of neural tissue, changes in blood vessels or signal quality, the end result is that aging does seem to affect estimates of SD-OCT RNFL thickness in longitudinal studies, as shown by Wu et al.[12] In our study, approximately one quarter of the variability in chronological age could be explained by the DL model using only RNFL.

Therefore it still seems important to take aging into account when using SD-OCT for glaucoma diagnosis and assessment of progression.

Other than the RNFL, the DL models using ablated images all had a similar performance in predicting age. When applied to the combined retinal layers excluding RNFL, the correlation was 0.672 ($R^2 = 45\%$), whereas the model applied to the choroid only had correlation of 0.736 ($R^2 = 54\%$), which was similar to the model using the vitreous and vitreoretinal interface ($r = 0.736$, $R^2 = 54\%$). All of these structures have been previously described to suffer age-related anatomical changes. Choroidal thickness has been shown to progressively decrease with normal aging.[15,16] Senescent microstructural changes in all layers of the human retina have been previously reported, such as thickening of the internal limiting membrane, decrease of retinal pigment epithelial cells density, as well as loss of photoreceptors.[17,44,45] With aging, the vitreous body suffers gradual liquefaction which may lead to separation from the internal limiting membrane of the retina, causing posterior vitreous detachment which can often be visualized on SD-OCT.[46–49]

One could argue that training separate DL models on the ablated images could lead to differences in performance related to the model characteristics themselves, rather than actual differences related to the specific anatomic structures. We therefore rerun our analyses by using only the original model trained on the whole image and applying it without modification to predict age on the ablated images. The results showed much lower predictive ability for all structures, including vitreous ($r = 0.137$, $R^2 = 1.9\%$), RNFL ($r = 0.037$, $R^2 = 0.1\%$), retinal layers excluding RNFL ($r = 0.102$, $R^2 = 1\%$) and choroid ($r = 0.258$, $R^2 = 6.7\%$). This result seems to indicate that age predictions of the original model used a combination of information derived from several different regions of the scan.

Our study had limitations. We only had cross-sectional data and the inter-subject variability may have made it difficult to evaluate subtle age-related changes that might occur over time in an individual. Longitudinal deep learning studies will be important to clarify this. As another limitation, we used only peripapillary RNFL scans. Our choice was due to the lack of available data from other scanning areas, but future studies could be directed at investigating aging effects on the macula and optic nerve head scans using a similar methodology. Axial length has also been shown to influence RNFL thickness and optic nerve head parameters from OCT, and further studies should investigate whether adding it as a feature could improve DL algorithm's accuracy for age estimation. The use of other techniques such as OCT angiography may also help to clarify the effects of aging on blood vessels as well.

In conclusion, a DL model applied to SD-OCT peripapillary scans was able to predict an individual's chronological age with high accuracy. The collective information gathered from the DL models applied to the whole scan and to specific retinal areas through image ablation suggests that the effect of aging occurs diffusely in many anatomical regions and is not primarily due to RNFL changes. Future longitudinal studies should be conducted to provide further clarification on the effects of aging on retinal tissues.

Acknowledgments

References

1. Huang D, Swanson EA, Lin CP, et al. Optical coherence tomography. *Science.* 1991;254(5035): 1178–1181.

2. Medeiros FA, Zangwill LM, Alencar LM, Sample PA, Weinreb RN. Rates of progressive retinal nerve fiber layer loss in glaucoma measured by scanning laser polarimetry. *Am J Ophthalmol.* 2010;149(6):908–915.

3. Chauhan BC, Hutchison DM, Artes PH, et al. Optic disc progression in glaucoma: comparison of confocal scanning laser tomography to optic disc photographs in a prospective study. *Invest Ophthalmol Vis Sci.* 2009;50(4):1682–1691.

4. Bussel II, Wollstein G, Schuman JS. OCT for glaucoma diagnosis, screening and detection of glaucoma progression. *Br J Ophthalmol.* 2014;98(Suppl 2):ii15–ii19.

5. Weinreb RN, Khaw PT. Primary open-angle glaucoma. *Lancet.* 2004;363(9422):1711–1720.

6. Alamouti B, Funk J. Retinal thickness decreases with age: an OCT study. *Br J Ophthalmol.* 2003;87(7):899–901.

7. Budenz DL, Anderson DR, Varma R, et al. Determinants of normal retinal nerve fiber layer thickness measured by Stratus OCT. *Ophthalmology.* 2007;114(6):1046–1052.

8. Kanamori A, Escano MF, Eno A, et al. Evaluation of the effect of aging on retinal nerve fiber layer thickness measured by optical coherence tomography. *Ophthalmologica.* 2003;217(4):273–278.

9. Vianna JR, Danthurebandara VM, Sharpe GP, et al. Importance of normal aging in estimating the rate of glaucomatous neuroretinal rim and retinal nerve fiber layer loss. *Ophthalmology.* 2015;122(12):2392–2398.

10. Parikh RS, Parikh SR, Sekhar GC, Prabakaran S, Babu JG, Thomas R. Normal age-related decay of retinal nerve fiber layer thickness. *Ophthalmology.* 2007;114(5):921–926.

11. Sung KR, Wollstein G, Bilonick RA, et al. Effects of age on optical coherence tomography measurements of healthy retinal nerve fiber layer, macula, and optic nerve head. *Ophthalmology.* 2009;116(6):1119–1124.

12. Wu Z, Saunders LJ, Zangwill LM, Daga FB, Crowston JG, Medeiros FA. Impact of normal aging and progression definitions on the specificity of detecting retinal nerve fiber layer thinning. *Am J Ophthalmol.* 2017;181:106–113.

13. Leung CK, Yu M, Weinreb RN, et al. Retinal nerve fiber layer imaging with spectral-domain optical coherence tomography: a prospective analysis of age-related loss. *Ophthalmology.* 2012;119(4):731–737.

14. Patel NB, Lim M, Gajjar A, Evans KB, Harwerth RS. Age-associated changes in the retinal nerve fiber layer and optic nerve head. *Invest Ophthalmol Vis Sci.* 2014;55(8):5134–5143.

15. Margolis R, Spaide RF. A pilot study of enhanced depth imaging optical coherence tomography of the choroid in normal eyes. *Am J Ophthalmol.* 2009;147(5):811–815.

16. Ramrattan RS, van der Schaft TL, Mooy CM, de Bruijn WC, Mulder PG, de Jong PT. Morphometric analysis of Bruch's membrane, the choriocapillaris, and the choroid in aging. *Invest Ophthalmol Vis Sci.* 1994;35(6):2857–2864.

17. Grossniklaus HE, Nickerson JM, Edelhauser HF, Bergman LA, Berglin L. Anatomic alterations in aging and age-related diseases of the eye. *Invest Ophthalmol Vis Sci.* 2013;54(14):ORSF23–ORSF27.

18. LeCun Y, Bengio Y, Hinton G. Deep learning. *Nature.* 2015;521(7553):436–444.

19. Shen D, Wu G, Suk HI. Deep learning in medical image analysis. *Annu Rev Biomed Eng.* 2017;19(1):221–248.

20. Poplin R, Varadarajan AV, Blumer K, et al. Prediction of cardiovascular risk factors from retinal fundus photographs via deep learning. *Nat Biomed Eng.* 2018;2(3):158–164.

21. Gulshan V, Peng L, Coram M, et al. Development and validation of a deep learning algorithm for detection of diabetic retinopathy in retinal fundus photographs. *JAMA.* 2016;316(22):2402–2410.

22. Ting DSW, Cheung CY, Lim G, et al. Development and validation of a deep learning system for diabetic retinopathy and related eye diseases using retinal images from multiethnic populations with diabetes. *JAMA.* 2017;318(22):2211–2223.

23. Phene S, Dunn RC, Hammel N, et al. Deep learning and glaucoma specialists: the relative importance of optic disc features to predict glaucoma referral in fundus photographs. *Ophthalmology.* 2019;126(12):1627–1639.

24. Jammal AA, Thompson AC, Mariottoni EB, et al. Human versus machine: comparing a deep learning algorithm to human gradings for detecting glaucoma on fundus photographs. *Am J Ophthalmol.* 2020;211:123–131.

25. Mariottoni EB, Jammal AA, Urata CN, et al. Quantification of retinal nerve fibre layer thickness on optical coherence tomography with a deep learning segmentation-free approach. *Sci Rep.* 2020;10(1):402.

26. Thompson AC, Jammal AA, Berchuck SI, Mariottoni EB, Medeiros FA. Assessment of a segmentation-free deep learning algorithm for diagnosing glaucoma from optical coherence tomography scans. *JAMA Ophthalmol.* 2020;138(4):333–339.

27. Shen D, Wu G, Suk HI. Deep learning in medical image analysis. *Annu Rev Biomed Eng.* 2017;19:221–248.

28. Heidelberg Engineering. Glaucoma Premium Edition. Available at: http://www.heidelberg engineering.com/. Accessed July 7, 2020.

29. Leite MT, Rao HL, Zangwill LM, Weinreb RN, Medeiros FA. Comparison of the diagnostic accuracies of the Spectralis, Cirrus, and RTVue optical coherence tomography devices in glaucoma. *Ophthalmology.* 2011;118(7):1334–1339.

30. Wu H, de Boer JF, Chen TC. Diagnostic capability of spectral-domain optical coherence tomography

for glaucoma. *Am J Ophthalmol.* 2012;153(5):815–826.e812.

31. He K, Zhang X, Ren S, Sun J. Deep residual learning for image recognition. Proceedings of the 2016 IEEE Conference on Computer Vision and Pattern Recognition (CVPR); 2016;770–778.

32. Russakovsky O, Deng J, Su H, et al. ImageNet Large Scale Visual Recognition Challenge. *Int J Comp Vis.* 2015;115(3):211–252.

33. Kingma DP, Ba J. Adam: a method for stochastic optimization. arXiv preprint arXiv:1412.6980. 2014.

34. Ruder S. An overview of gradient descent optimization algorithms. arXiv preprint arXiv:1609.04747. 2016.

35. Smith LN. Cyclical learning rates for training neural networks. *2017 IEEE Winter Conference on Applications of Computer Vision (WACV).* 2017:464–472.

36. Selvaraju RR, Cogswell M, Das A, Vedantam R, Parikh D, Batra D. Grad-CAM: visual explanations from deep networks via gradient-based localization. *2017 Ieee International Conference on Computer Vision (ICCV).* 2017:618–626.

37. Medeiros FA, Sample PA, Zangwill LM, Liebmann JM, Girkin CA, Weinreb RN. A statistical approach to the evaluation of covariate effects on the receiver operating characteristic curves of diagnostic tests in glaucoma. *Invest Ophthalmol Vis Sci.* 2006;47(6):2520–2527.

38. Liang KY, Zeger SL. Longitudinal Data-Analysis Using Generalized Linear-Models. *Biometrika.* 1986;73(1):13–22.

39. Fortune B, Reynaud J, Cull G, Burgoyne CF, Wang L. The effect of age on optic nerve axon counts, SDOCT Scan quality, and peripapillary retinal nerve fiber layer thickness measurements in Rhesus monkeys. *Transl Vis Sci Technol.* 2014;3(3):2–2.

40. Balazsi AG, Rootman J, Drance SM, Schulzer M, Douglas GR. The effect of age on the nerve fiber population of the human optic nerve. *Am J Ophthalmol.* 1984;97(6):760–766.

41. Mikelberg FS, Drance SM, Schulzer M, Yidegiligne HM, Weis MM. The normal human optic nerve. Axon count and axon diameter distribution. *Ophthalmology.* 1989;96(9):1325–1328.

42. Johnson BM, Miao M, Sadun AA. Age-related decline of human optic nerve axon populations. *AGE.* 1987;10(1):5–9.

43. Jonas JB, Schmidt AM, Müller-Bergh JA, Schlötzer-Schrehardt UM, Naumann GO. Human optic nerve fiber count and optic disc size. *Invest Ophthalmol Vis Sci.* 1992;33(6):2012–2018.

44. Gao H, Hollyfield JG. Aging of the human retina. Differential loss of neurons and retinal pigment epithelial cells. *Invest Ophthalmol Vis Sci.* 1992;33(1):1–17.

45. Panda-Jonas S, Jonas JB, Jakobczyk-Zmija M. Retinal photoreceptor density decreases with age. *Ophthalmology.* 1995;102(12):1853–1859.

46. Sebag J. Age-related changes in human vitreous structure. *Graefes Arch Clin Exp Ophthalmol.* 1987;225(2):89–93.

47. Los LI, van der Worp RJ, van Luyn MJ, Hooymans JM. Age-related liquefaction of the human vitreous body: LM and TEM evaluation of the role of proteoglycans and collagen. *Invest Ophthalmol Vis Sci.* 2003;44(7):2828–2833.

48. Asrani S, Essaid L, Alder BD, Santiago-Turla C. Artifacts in spectral-domain optical coherence tomography measurements in glaucoma. *JAMA Ophthalmol.* 2014;132(4):396–402.

49. Liu Y, Baniasadi N, Ratanawongphaibul K, Chen TC. Effect of partial posterior vitreous detachment on spectral-domain optical coherence tomography retinal nerve fibre layer thickness measurements. *Br J Ophthalmol.* 2020;104(11):1524–1527.